Hindawi Publishing Corporation
Journal of Nanomaterials
Volume 2015, Article ID 215371, 10 pages
http://dx.doi.org/10.1155/2015/215371

Research Article

$CaCl_2$-Accelerated Hydration of Tricalcium Silicate: A STXM Study Combined with ^{29}Si MAS NMR

Qinfei Li,[1,2] Yong Ge,[1] Guoqing Geng,[2] Sungchul Bae,[2,3] and Paulo J. M. Monteiro[2]

[1]*School of Transportation Science and Engineering, Harbin Institute of Technology, Harbin 150090, China*
[2]*Department of Civil and Environmental Engineering, University of California at Berkeley, Berkeley, CA 94720, USA*
[3]*Faculty of Science and Technology, Tokyo University of Science, 2641 Yamasaki, Noda, Chiba 278-8510, Japan*

Correspondence should be addressed to Qinfei Li; hitqfli@gmail.com

Received 20 August 2015; Revised 5 November 2015; Accepted 16 November 2015

Academic Editor: Jin-Ho Choy

The effect of calcium chloride ($CaCl_2$) on tricalcium silicate (C_3S) hydration was investigated by scanning transmission X-ray microscopy (STXM) with Near Edge X-ray Absorption Fine Structure (NEXAFS) spectra and ^{29}Si MAS NMR. STXM is demonstrated to be a powerful tool for studying the chemical composition of a cement-based hydration system. The Ca $L_{3,2}$-edge NEXAFS spectra obtained by examining C_3S hydration in the presence of $CaCl_2$ showed that this accelerator does not change the coordination of calcium in the calcium silicate hydrate (C-S-H), which is the primary hydration product. O K-edge NEXAFS is also very useful in distinguishing the chemical components in hydrated C_3S. Based on the Ca $L_{3,2}$-edge spectra and chemical component mapping, we concluded that $CaCl_2$ prefers to coexist with unhydrated C_3S instead of C-S-H. In Si K-edge NEXAFS analysis, $CaCl_2$ increases the degree of silicate polymerization of C-S-H in agreement with the ^{29}Si CP/MAS NMR results, which show that the presence of $CaCl_2$ in hydrated C_3S considerably accelerates the formation of middle groups (Q^2) and branch sites (Q^3) in the silicate chains of C-S-H gel at 1-day hydration.

1. Introduction

Calcium chloride ($CaCl_2$) plays an important role in accelerating the hydration and setting of tricalcium silicate (C_3S) and Portland cement [1–3]. $CaCl_2$ has been used widely in construction using unreinforced concrete [3] due to steel corrosion. The rate of formation of hydration products has often been observed to increase in the presence of $CaCl_2$, thereby accelerating the rate of heat evolution during hydration [1, 3]. This accelerating admixture promotes the dissolution of the cations or anions from the cement, thereby accelerating the growth rate of calcium silicate hydrate (C-S-H), which is a complicated physical and chemical process for nucleation and growth [4]. However, this mechanism is not fully understood at the molecular level [5].

The microstructure and nanostructure of the hydration products are expected to be influenced by speeding up the hydration reaction. $CaCl_2$ is well known to have the ability to increase the nitrogen surface area and pore volume of Portland cement and C_3S pastes [6, 7]. The "sheaf-of wheat" or fibrous morphology of hydrated C_3S in the presence of $CaCl_2$ has been investigated using various microscopy techniques [2, 8–11], such as scanning electron microscopy (SEM), transmission electron microscopy (TEM), and full-view transmission soft X-ray microscopy, but little information has been obtained about the chemical and physical properties corresponding to the morphology. Transmission soft X-ray microscopy has increasingly been utilized in exploring the cement-based materials [2, 8, 12, 13]. Juenger et al. [2] found that $CaCl_2$ accelerates the formation of "inner product" C-S-H with a low-density microstructure. The C-S-H is formed early and outside the original grain boundary as bridge spaces between grains. Thomas et al. studied the development of the microstructure and kinetics of pure C_3S and $CaCl_2$-accelerated C_3S pastes, and they reported that $CaCl_2$ accelerated the rate of nucleation of the hydration product on the surface of the C_3S particles significantly but that $CaCl_2$ has relatively little effect on the growth rate [1]. These studies demonstrated that both morphologic information about hydrated C_3S in the presence of $CaCl_2$

and exploration of chloride binding are needed. However, the analytical approaches listed above have certain limitations in that they do not include the chemical speciation of elements in heterogeneous materials on the submicron-scale.

Scanning transmission X-ray microscopy (STXM) provides information on both morphology and X-ray Absorption Spectroscopy (XAS). STXM is a promising technique in further understanding the structure and properties of the C-S-H phase [14–19]. The STXM technique allows the investigation of amorphous and crystalline materials. In addition to obtaining the chemical speciation information, STXM allows the identification of heterogeneity within the samples on a particle-by-particle basis. Significantly, image stacks (where a series of images is collected corresponding to each energy level observed by STXM with Near Edge X-ray Absorption Fine Structure (NEXAFS)) were converted into chemical component mapping. The results can be visualized by RGB overlay maps using Singular Value Decomposition (SVD) based on reference spectra [20]. Because various chemical components have unique NEXAFS spectra, the reference spectra obtained from known components were used to visualize and differentiate phases in a sample [21].

To investigate the effects of $CaCl_2$ on the microstructure of hydration products during the hydration of C_3S, X-ray diffraction (XRD), ^{29}Si MAS NMR, and scanning transmission X-ray microscopy (STXM) measurements were taken to investigate the interactions between calcium chloride and C-S-H. Through the use of STXM in combination with concurrent measurements of NEXAFS, the results from this study will examine sample composition and spatial heterogeneities and thus aid in explaining the interactions between calcium or chloride ions and C-S-H. This will improve understanding of the accelerating role of $CaCl_2$ on the chemical information of C-S-H, bringing the state of the art a step closer to the development of admixtures for advanced concrete structures.

2. Materials and Methods

2.1. Materials. Triclinic C_3S passing through sieve #325 (45 μm) was purchased from CTL Group (Skokie, IL). Finely ground anhydrous triclinic C_3S powder was mixed with a 0.1 M $CaCl_2$ solution with a liquid-to-solid ratio of 1.0. A C_3S paste produced for STXM was maintained in CryoTube vials (1.8 mL) under the protection of N_2 gas at room temperature and was then sealed in a vacuum bag. After a period of hydration of 1, 3, 7, and 28 d, samples of hydrated C_3S with an addition of $CaCl_2$ were dried in a vacuum oven at 23°C before X-ray diffraction and ^{29}Si MAS NMR measurements.

2.2. X-Ray Diffraction. Samples of hydrated C_3S with an addition of $CaCl_2$ at different hydration times were tested using a PANalytical X'Pert Pro diffractometer equipped with a Co X-ray tube (λ = 1.79 Å) and the rapid X'celerator detector. The XRD patterns of the samples were analyzed using the X-Pert High Score Plus software. XRD was used to identify crystalline phases from a 2θ value of 5–55° with a step of 0.02°.

2.3. Scanning Transmission X-Ray Microscopy. After 7 d of hydration, the C_3S paste was ground and dispersed with deionized water for STXM measurement. A drop of 0.1 μL of C_3S solution was taken and placed on the center of the Si_3N_4 membrane window (core: 1 mm × 1 mm × 100 nm; frame: 5 mm × 5 mm × 0.2 mm) with a micropipette. Residual water was removed from the window.

The reference Ca $L_{3,2}$-edge NEXAFS spectra of $CaCl_2$ particles on the Si_3N_4 window were also measured. STXM experiments were performed at the Advanced Light Source (ALS) at Lawrence Berkeley National Laboratory (LBNL) beamline 5.3.2.1 (700–2500 eV) and beamline 5.3.2.2 (250–800 eV) [23]. The images and NEXAFS spectra of the Ca $L_{3,2}$-edge (340–360 eV), O K-edge (520–560 eV), and Si K-edge (1825–1890 eV) were measured. The Axis 2000 software (version 2.1) was used to align stack images and extract NEXAFS spectra from the stack and line scan images. The stack scan collects absorption data for the field of view at each preselected energy point.

2.4. ^{29}Si MAS NMR. Solid-state NMR spectra were recorded on a Bruker MSL-300 spectrometer in which the resonance frequency for ^{29}Si is 59.63 MHz. Samples were packed into a 4 mm Zirconia rotor. High-power proton decoupling was used for the ^{29}Si spectra, and chemical shifts are quoted relative to external tetramethylsilane (TMS) for ^{29}Si. Typical acquisition parameters for recording the ^{29}Si spectra were a 4.5 kHz sample spinning speed, 4 μs pulse length, and 6 KHz sweep width. ^{29}Si cross-polarization magic-angle spinning (CPMAS) experiments were performed using a relaxation delay of 12 μs.

3. Results and Discussion

3.1. XRD Patterns. The results of the XRD analysis of the chloride-containing samples with different hydration times are shown in Figure 1. Portlandite crystals ($Ca(OH)_2$) and unhydrated C_3S can be observed starting at 1 d of hydration. At 28 d, unhydrated C_3S was no longer observed. Due to the poor crystallinity of amorphous C-S-H, there is just a hump associated with the formation of C-S-H at a d-spacing of 3.08 Å starting at 3 d for hydrated C_3S with $CaCl_2$.

3.2. Ca $L_{3,2}$-Edge NEXAFS Analysis. The references of unhydrated C_3S, pure $Ca(OH)_2$, and pure C-S-H were first determined by Bae et al. [22], whereas the reference for $CaCl_2$ was collected in the present study. C_3S and its hydration products are calcium compounds. Ca $L_{3,2}$-edge NEXAFS spectra provide a calcium coordination environment and conveniently characterize the amorphous and crystalline Ca-containing materials that are present in these reference compounds and 7-day-hydrated C_3S with $CaCl_2$ in Figure 2. The observed multiple peak patterns of Ca $L_{3,2}$-edge NEXAFS spectra consist of two main spin-orbit related peaks (a_2 and b_2) corresponding to L_3 and L_2, along with several smaller peaks (a_1 and b_1) leading to the main peaks (Figure 2). The experimental resolution for the spectra is less than approximately 0.1 eV. The magnitudes and symmetry of

Table 1: Peak positions and splitting energy values of the reference Ca $L_{3,2}$-edge and the different areas of the C_3S particles in the presence of $CaCl_2$.

Samples	Peak positions (ev)				ΔCa-$L_3(a_2 - a_1)$	ΔCa-$L_2(b_2 - b_1)$
	a_1	a_2	b_1	b_2		
$CaCl_2$-ref	348.0	349.2	351.3	352.4	1.2	1.1
$Ca(OH)_2$-ref*	347.6	349.1	351.0	352.4	1.5	1.4
Unhydrated C_3S-ref*	347.7	349.0	351.1	352.3	1.3	1.2
C-S-H-ref*	348.1	349.1	351.4	352.4	1.0	1.0
Area 1	347.7	349.0	351.1	352.3	1.3	1.2
Area 2	347.9	348.9	351.2	352.3	1.0	1.1
Area 3	347.8	349.0	351.1	352.3	1.2	1.2

*Data from Bae et al. [22].

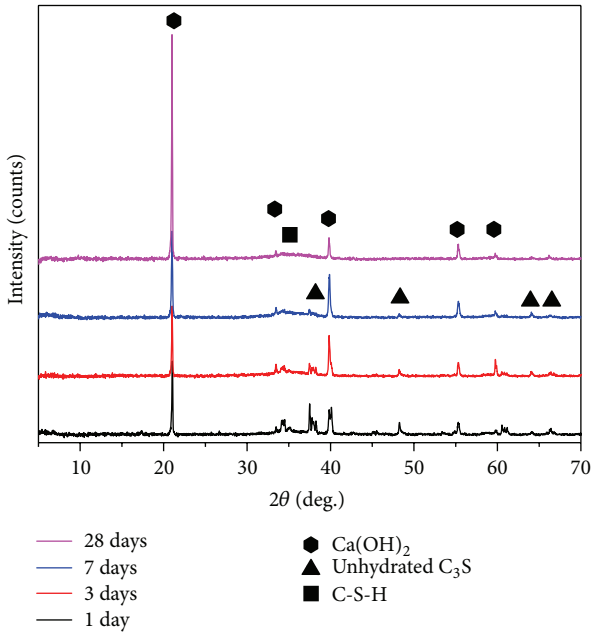

Figure 1: XRD patterns of phase changes from hydrated C_3S in the presence of $CaCl_2$ at different hydration times.

the crystal field of calcium in the first coordination sphere result in crystal field splitting, which is the origin of these multipeak patterns. The peak positions and energy separation values ($\Delta L_3(a_2 - a_1)$ and $\Delta L_2(b_2 - b_1)$) are related to the symmetry of Ca^{2+}, given in Table 1.

Figure 2 presents the Ca $L_{3,2}$-edge NEXAFS spectra of $CaCl_2$, $Ca(OH)_2$, pure C-S-H, and anhydrous C_3S as the references. Each of these spectra is unique in terms of its shape and peak positions as well as the splitting shown in Table 1. The uniqueness of each spectrum has been used as a fingerprint for investigating the Ca structure. The larger splitting energy and peak intensity ratio in the Ca $L_{3,2}$-edge NEXAFS spectra are good indications of the well-developed crystalline Ca structure, which means that the splitting energy values for $\Delta(a_2 - a_1)$ and $\Delta(b_2 - b_1)$ are nonlinearly related to the value of the crystal field parameter (10 Dq). $Ca(OH)_2$, with octahedral symmetry (O_h) [24], shows larger splitting energy values and peak intensity ratios for a_1/a_2 and b_1/b_2 compared with the values and ratios of unhydrated C_3S and pure C-S-H due to the different electronegativity in the crystal field. The reference of pure C-S-H in 17-day-hydrated C_3S [22] has the smallest splitting energy and peak intensity ratio shown in Figure 2, which result from its amorphous or poor-crystallinity structure. In addition, the peak intensity ratios for a_1/a_2 and b_1/b_2 generally indicate the magnitude of the crystal field and suggest that C-S-H has the smallest crystal field parameter but that $CaCl_2$ has the largest. The mean coordination number of $CaCl_2$ is six in the octahedral crystal field (positive) [25].

3.3. STXM Analysis of 7-Day-Hydrated C_3S with $CaCl_2$. The selected areas of a 7-day-hydrated C_3S particle in the presence of $CaCl_2$ were analyzed by Ca $L_{3,2}$-edge and O K-edge NEXAFS spectroscopy, as shown in Figure 2. The peak positions, splitting energy values, and references of Ca $L_{3,2}$-edge NEXAFS spectra are listed in Table 1. In Figure 2(d), Ca $L_{3,2}$-edge NEXAFS for Area 1 has the largest splitting energy and peak intensity ratio, and Area 2 has the smallest. The peak positions for Area 2 shift slightly by approximately −0.2 eV, but the splitting energy for Area 2 is similar to that of the C-S-H reference. The energy separation of C-S-H with 1.0 and 1.1 for $\Delta(a_2 - a_1)$ and $\Delta(b_2 - b_1)$ and the smallest peak intensity ratios for a_1/a_2 and b_1/b_2 in Area 2 suggest that the calcium in C-S-H has a randomly spherical coordination with the oxygen, which means that the coordination environment of calcium in C-S-H is asymmetric. This observation suggests that $CaCl_2$ does not change the coordination environment of calcium in C-S-H. Moreover, the energy separation of Area 3, with 1.2 and 1.2 for $\Delta(a_2 - a_1)$ and $\Delta(b_2 - b_1)$, respectively, is similar to that of the unhydrated C_3S reference. Therefore, these areas are identified by Ca $L_{3,2}$-edge NEXAFS spectra, which are compared with the peak positions, splitting energy, and peak shape of the above references: Area 1 is related to $Ca(OH)_2$, Area 2 is related to C-S-H, and Area 3 is related to unhydrated C_3S.

We also present the O K-edge NEXAFS spectroscopy of the three areas in the same particle shown in Figure 2(e). The O K-edge NEXAFS spectrum can provide simultaneous chemical information about hydration products and unhydrated C_3S and shows that the differences in the O K-edge NEXAFS spectra are sufficiently significant to distinguish the distinct hydration products.

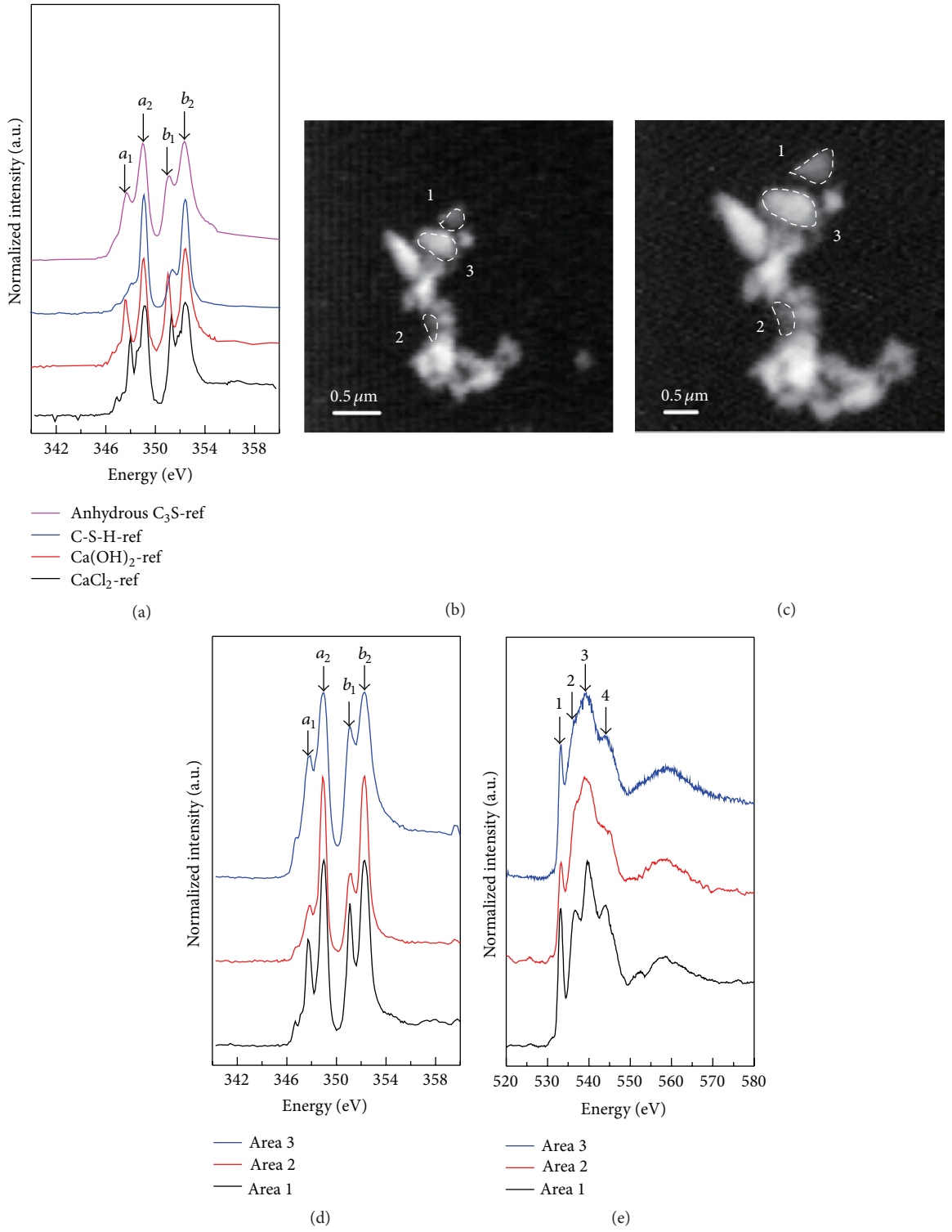

FIGURE 2: (a) Ca $L_{3,2}$-edge NEXAFS spectra of the reference anhydrous C_3S^*, C-S-H^*, $Ca(OH)_2{}^*$, and $CaCl_2$ (∗ data from Bae et al. [22]), (b) and (c) a single image of 7-day-hydrated C_3S in the presence of $CaCl_2$ taken at, respectively, 340 eV and 525 eV, (d) Ca $L_{3,2}$-edge NEXAFS spectra of the selected area in (b), and (e) O K-edge NEXAFS spectra of the selected area in (c).

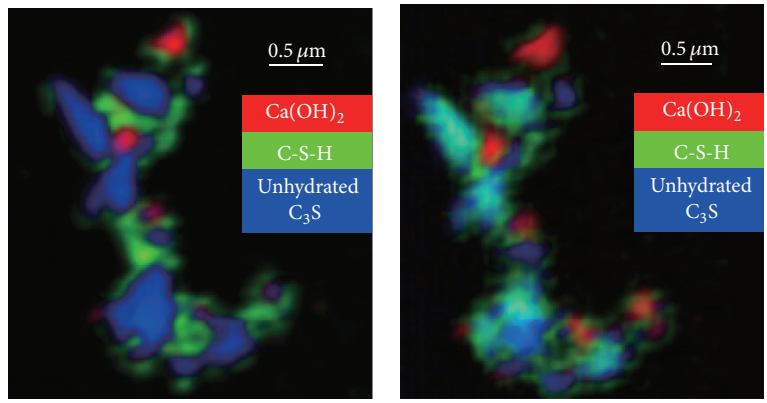

(a) (b)

FIGURE 3: Decomposition diagram of RGB overlay maps using SVD for the C_3S particle in the presence of $CaCl_2$ based on NEXAFS spectra obtained from the reference in Figure 2 and the different areas in Figure 3: (a) Ca $L_{3,2}$-edge image stacks; (b) O K-edge image stacks.

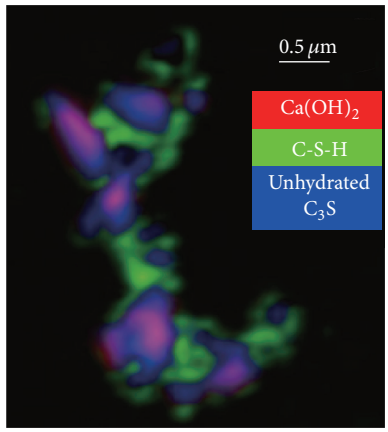

FIGURE 4: Decomposition diagram of RGB overlay maps using SVD for the C_3S particle in the presence of $CaCl_2$ based on the Ca $L_{3,2}$-edge NEXAFS spectra obtained from the reference in Figure 2 and the different areas in Figure 3.

In Figure 2(e), there are four peaks, labeled 1 through 4, in each O spectrum. Peak 1 is a π^* peak, and peaks 3 and 4 are σ^* peaks. However, peak 2 behaves differently across different types of crystallinity [26]. Peak 2 is sharper in $Ca(OH)_2$ than are the peaks in C-S-H and in unhydrated C_3S. The layered crystal structure of Portlandite ($Ca(OH)_2$) is well known to be trigonal with the space group $P\bar{3}m1$ and can be described as stacked sheets of distorted edge-sharing Ca-O octahedra along the *c*-axis [27]. Each hydroxyl group is coordinated by three Ca atoms in its layer and is surrounded by three other hydroxyl groups that belong to the adjacent layer. Unhydrated C_3S is triclinic and consists of the mean coordination number (6.21) [28] of Ca cations and the SiO_4 tetrahedra, which show varying degrees of disorder. Therefore, there are weaker π^* peaks, and peak 2 in the O K-edge NEXAFS of C-S-H is due to the poor crystallization of C-S-H.

Image stacks, where a series of images is collected corresponding to each energy, were collected to convert into chemical component mapping. As shown in Figure 3, the results were visualized by RGB overlay maps using Singular Value Decomposition (SVD) based on reference spectra [20]. Because various chemical components have unique NEXAFS spectra, the reference spectra obtained from known components were used to visualize and differentiate phases in a sample [21]. Both of the distributions of phases in the same hydrated C_3S in the presence of $CaCl_2$ with the Ca $L_{3,2}$-edge and the O K-edge image stacks are presented in Figure 3. We observe a few magenta pixels (M = R + B = $Ca(OH)_2$ + unhydrated C_3S) in Figure 3. There are, however, numerous cyan pixels (C = G + B = C-S-H + unhydrated C_3S) in Figure 3(b), which indicate unhydrated C_3S in those pixels is transforming to C-S-H; however, there are a few yellow pixels (Y = R + G = $Ca(OH)_2$ + C-S-H). Clearly, the C-S-H surrounds the unhydrated C_3S, along with the formation of $Ca(OH)_2$. Obviously, the RGB overlay map based on the O K-edge image stacks is similar to the RGB overlay map based on the Ca $L_{3,2}$-edge image stacks. However, in the case of the O K-edge image stacks, the morphology of the C-S-H gel was more present in the details where the flocculent C-S-H gel surrounds the unhydrated C_3S and $Ca(OH)_2$, in good accordance with the results for Ca $L_{3,2}$-edge.

Because RGB overlay maps using Singular Value Decomposition (SVD) can consist of no more than three components, the chemical component mapping for unhydrated C_3S, C-S-H, and $Ca(OH)_2$ are shown in Figure 3, and Figure 4 shows the RGB overlay maps with unhydrated C_3S, C-S-H gel, and $CaCl_2$. We observe numerous magenta pixels (M = R + B = $CaCl_2$ + unhydrated C_3S) even at the center of these unhydrated C_3S, which indicates that $CaCl_2$ diffuses into the inside of unhydrated C_3S during the transformation from unhydrated C_3S to C-S-H and $Ca(OH)_2$. Interestingly, the red part ($CaCl_2$) in Figure 4 was not intermingled with the green part, C-S-H gel, but instead with unhydrated C_3S. In other words, $CaCl_2$ coexists with unhydrated C_3S instead of C-S-H in the case of 7-day-hydrated C_3S with $CaCl_2$. Calcium chloride increases the dissolution of C_3S for easier diffusion of water into the hydrating particle and moves Ca^{2+} and

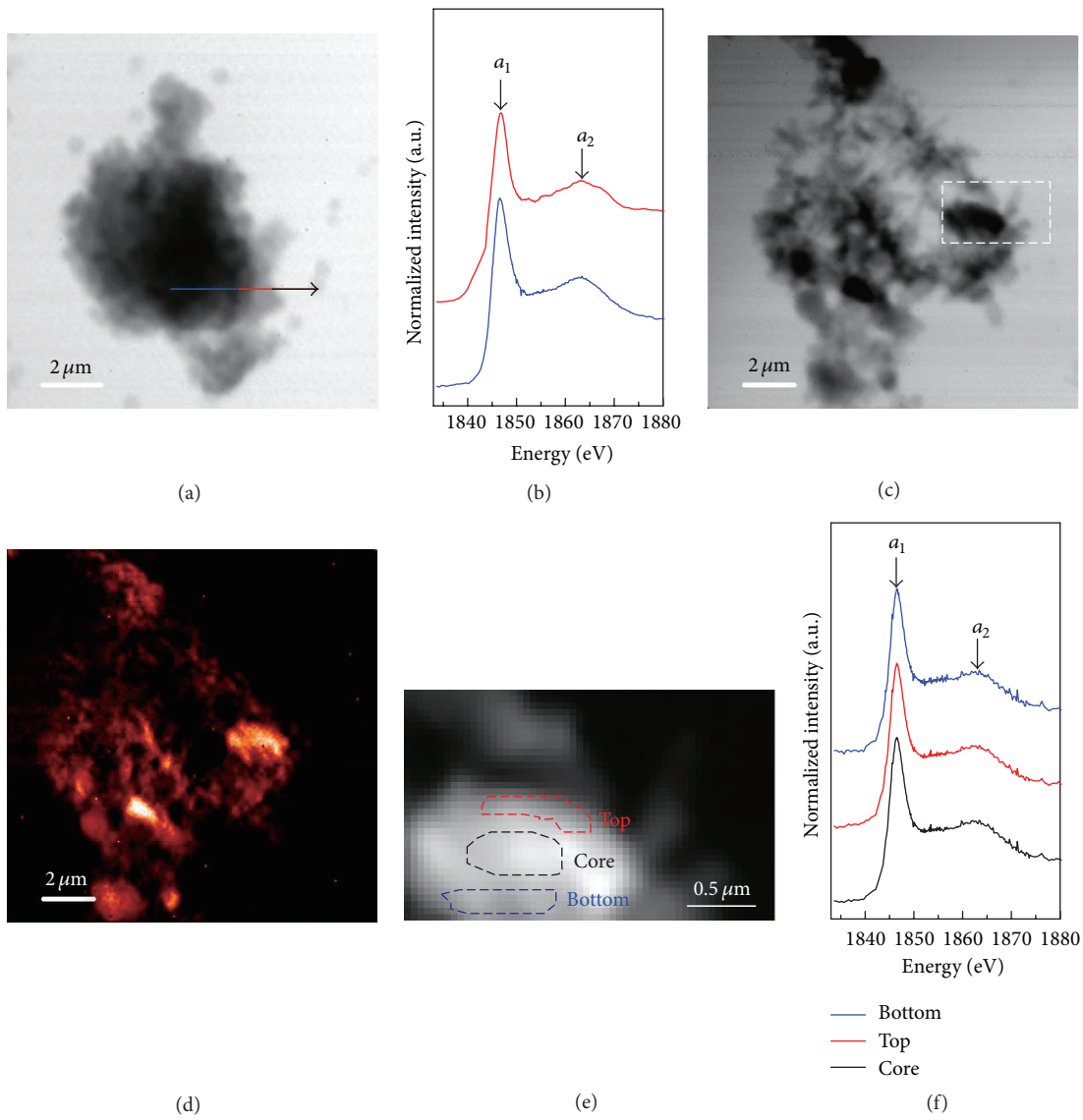

Figure 5: Si K-edge NEXAFS analysis of 7-day-hydrated C_3S particles in the presence of $CaCl_2$: (a) single image of one particle taken at 1855 eV, (b) Si K-edge NEXAFS spectra of the line-scan indicated in (a), (c) single image of another particle taken at 1855 eV, (d) image contrast mapping corresponding to (c), (e) selected areas in the image contrast map enlarged partly from (c) for the NEXAFS spectra, and (f) Si K-edge NEXAFS spectra taken from the different locations indicated in (e).

silicon ions away from the particle to form C-S-H gel and Portlandite [2].

The Si K-edge NEXAFS analysis on 7-day-hydrated C_3S in the presence of $CaCl_2$ is shown in Figure 5. The flocculent and the fibrillary hydration product can be observed, respectively, in Figures 3(a) and 3(b). The distribution map of silicon, as seen in Figure 5(d), is the computed optical density between the image taken at the preadsorption edge at 1830 eV and the near-adsorption edge at 1840 eV. With respect to the hydration of C_3S, $Ca(OH)_2$ contains no silicon, whereas the unhydrated C_3S and C-S-H have silicon-containing composition. Figures 5(b) and 5(f) show the Si K-edge NEXAFS spectra of the corresponding line-scan in Figure 5(a) and selected areas in Figure 5(e). Each spectrum consists of the main peak (a_1) and the multiple scattering peak (a_2). Peak a_1 is assigned to the transition of Si 1s electrons to the antibonding t_2 orbital (3p-like state), whereas peak a_2 is qualitatively attributable to the multiple scattering effect beyond the second coordination sphere [29].

The peak positions and energy separation ($\Delta a_2 - a_1$) shown in Table 2 are associated with the degree of polymerization in the silicates [22]. A line-scan on the flocculent particle shown in Figure 5(a) was selected to verify the changes from center to boundary, which had similar absorption features to synthetic C-S-H, with 0.66 and 0.95 Ca/Si ratios in previous studies [22]. Three locations (core, top, and bottom) were selected to verify the uniformity of the hydration product in Figure 5(e). These locations had no

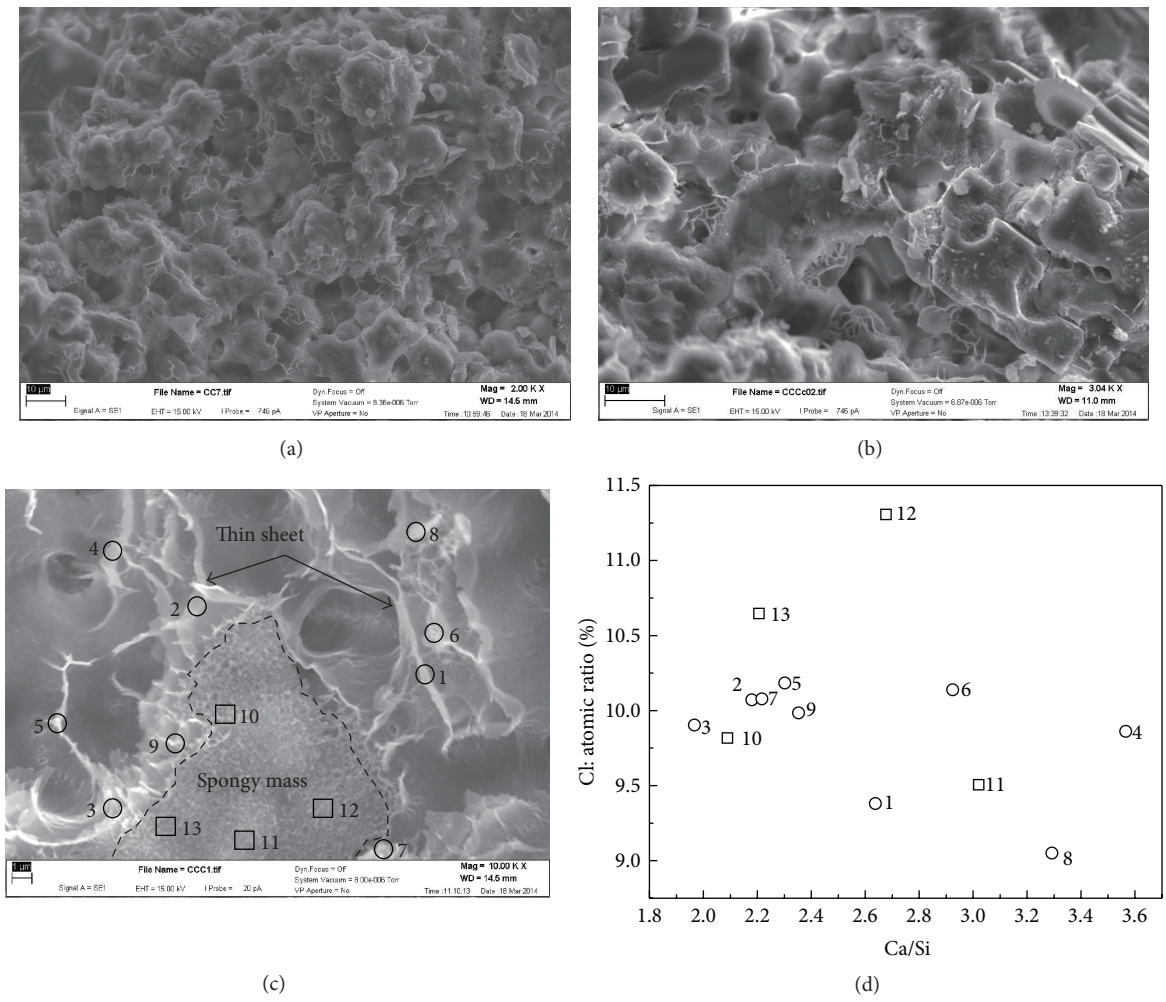

Figure 6: (a)~(c) The morphology of 7-day-hydrated C_3S in presence of $CaCl_2$ imaged by SEM, (d) SEM-EDS analysis of (c), Cl versus Ca/Si.

Table 2: Peak positions and the energy separation between peak positions of Si K-edge NEXAFS spectra of selected areas in 7-day-hydrated C_3S with $CaCl_2$ (C and Op denote the core area and outer product of C_3S, resp., in Bae et al. [22]).

	Peak a_1 (eV)	Peak a_2	$\Delta a_2 - a_1$
Blue line	1846.6	1863.2	16.6
Red line	1846.9	1863.0	16.1
Core	1846.5	1861.9	15.4
Top	1846.5	1861.9	15.4
Bottom	1846.5	1862.0	15.5
Anhydrous C_3S*	1847.7	1858.9	11.2
Syn-CSH0.66*	1846.9	1863.4	16.5
Syn-CSH0.95*	1846.7	1863.1	16.4
Syn-CSH1.44*	1846.4	1861.5	15.1
Op*	1847.4	1862.7	15.4
C*	1847.7	1559.4, 1861.5	11.4, 13.8

*Data from Bae et al. [22].

difference among their absorption features but were similar to Op and synthetic C-S-H, with a 1.44 Ca/Si ratio in previous studies [22]. Therefore, the hydration product of C_3S with $CaCl_2$ at 7 d in Figure 5(e) had a uniform degree of silicate polymerization. C_3S hydration is a dissolution-precipitation process [30]; however, $CaCl_2$ accelerated the rate of nucleation of the hydration product on the surface of the C_3S particles significantly, but $CaCl_2$ has relatively little effect on the growth rate [1]. Hence, after 7 d of hydration of C_3S with $CaCl_2$, the degree of silicate polymerization in the hydration product was close to that of the 17-day-hydrated C_3S in previous studies [22], thus implying that $CaCl_2$ increases the degree of silicate polymerization, especially in the case of Ip. Therefore, $CaCl_2$ can also facilitate ion diffusion [31], prompt the dissolution process of C_3S, and accelerate the formation of "inner product" C-S-H [2], ultimately resulting in a higher degree of silicate polymerization at either the core or the boundary of 7-day-hydrated C_3S.

The fracture surface of 7-day-hydrated C_3S in the presence of $CaCl_2$ imaged by SEM is shown in Figure 6. Thin-sheet C-S-H and the spongy mass C-S-H are observed in Figures 6(a)–6(c). "Honeycomb-like" morphologies of hydration products in the presence of $CaCl_2$ are shown at ages of 3 h to 7 d by SEM [32]. Because of the 0.1 M $CaCl_2$ used,

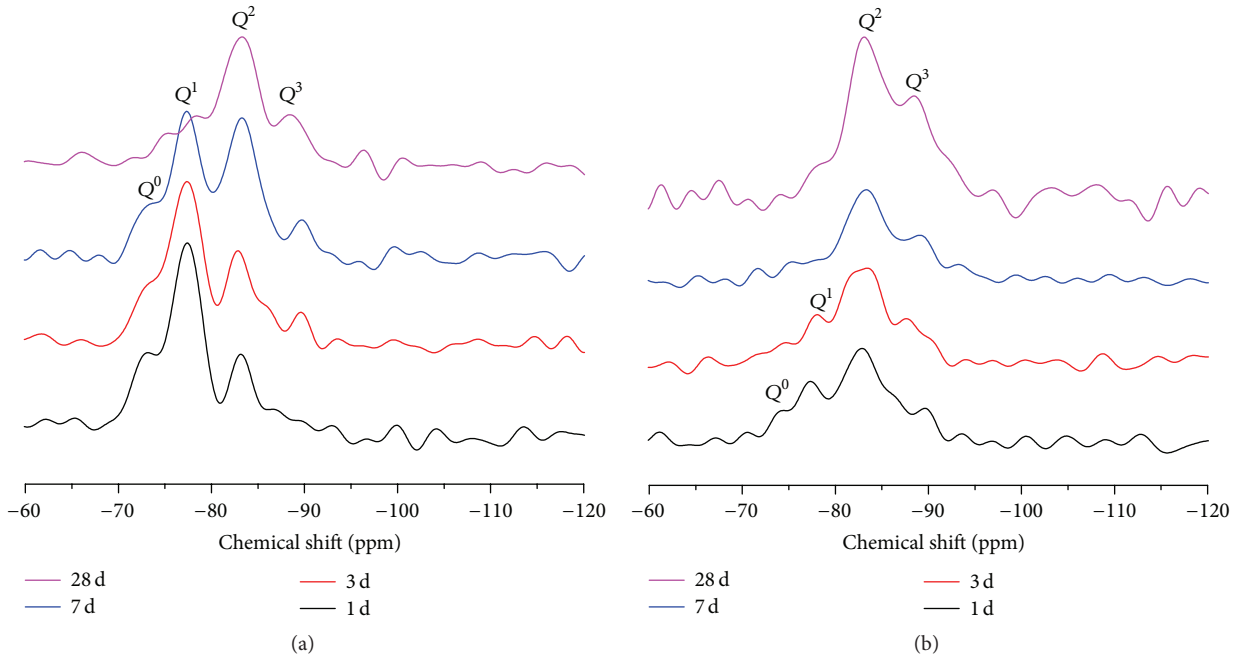

Figure 7: ^{29}Si CP/MAS NMR spectra of C_3S paste as a function of hydration time in the absence (a) and in the presence (b) of $CaCl_2$.

the Ca/Si ratio for the honeycomb C-S-H ranges between 2.0 and 3.6, whereas that for the spongy mass C-S-H is also included in the range. $CaCl_2$ accelerates the nucleation of the hydration product on the surface of the C_3S particles [1] and possibly prompts the bridge of the dreierketten silicate chains of C-S-H to develop in the two-dimensional direction into thin-sheet C-S-H.

3.4. ^{29}Si MAS NMR Analysis. ^{29}Si CP/MAS NMR was proven to be very useful for studying the chemical shifts of the corresponding element. The primary advantage of this method is its high resolution of signals, so the relationship between Si chemical shifts and corresponding assigned structure of silica unites is easy to establish. ^{29}Si CP/MAS NMR plots for hydrated C_3S with different hydration times in the absence or presence of $CaCl_2$ are shown in Figure 7. To describe various types of silica unites, we used Q^n ($n \leq 4$) for the connectivity of SiO_4 tetrahedra, where n represents the number of bridging oxygen (Si-O-Si): the Q^0 site is isolated SiO_4 tetrahedra, Q^1 is SiO_4 tetrahedra present in end unites of a silicate chain, Q^2 is a middle group, Q^3 is a branching site, and Q^4 sites link to four other SiO_4 tetrahedra in a three-dimensional network. Amorphous C-S-H initially contains mainly dimeric silicate [33–35], whereas C_3S includes nine inequivalent SiO_4 tetrahedra (Q^0 sites) between −69 ppm and −75 ppm [36]. In our analysis, the Gaussian distributions centered about −75 ppm, −78 ppm, −83 ppm, and −89 ppm are attributed, respectively, to Q^0, Q^1, Q^2, and Q^3 units [37, 38]. ^{29}Si CP/MAS NMR could not provide an accurate quantitative analysis of Q^n but instead indicated the chemical shift of the corresponding Q^n sites. However, for comparison, the trend for evaluating the fraction of Q^n could be reflected by ^{29}Si CP/MAS NMR.

Prior to the 7-day-hydration process of C_3S without $CaCl_2$, the discrete SiO_4 tetrahedra (Q^0) in unhydrated C_3S transformed to dominant dimers Q^1 and doubly coordinated tetrahedral Q^2 in the hydrated C_3S, while there was the occurrence of Q^3 at 3 days of hydration. However, the Q^0 and Q^1 peaks maintained the lowest level at 28 d, and the Q^2 peak became a predominant level. In the presence of $CaCl_2$, the Q^2 peak played a dominant role in the dreierketten silicate chain structure after 1 d of hydration, and the Q^3 peak at −89 ppm began to emerge compared with the control group, as shown. $CaCl_2$ is clearly indicated to considerably accelerate the formation of middle groups (Q^2) and branch sites (Q^3) in the silicate chains of C-S-H gel. $CaCl_2$ significantly accelerates the rate of nucleation of the hydration product deposited on the surface of the C_3S particles but has a relatively insignificant effect on the growth rate [1], thus explaining why the Q^2 peaks in the $CaCl_2$ group played a leading role in the dreierketten silicate chain structure. The earlier emergence of Q^2 and Q^3 peaks of the $CaCl_2$ group indicates that $CaCl_2$ accelerates the degree of silicate polymerization in hydrated C_3S in agreement with the above studies of the morphology of hydrated C_3S in the presence of $CaCl_2$. From the perspective of ionic diffusion, $CaCl_2$ cannot only facilitate diffusion of ions [31] but also prompt the dissolution process of C_3S and accelerate the formation of "inner product" C-S-H [2], along with a higher degree of silicate polymerization at either the core or the boundary of 7-day-hydrated C_3S.

4. Conclusions

Scanning transmission X-ray microscopy with NEXAFS spectra offers the possibility of studying the effect of $CaCl_2$ on the microstructure of hydration products. The chemical

composition information of the systems can easily be determined by STXM with NEXAFS.

The results from the Ca $L_{3,2}$-edge NEXAFS spectra of C_3S hydration in the presence of $CaCl_2$ show that $CaCl_2$ does not change the coordination of calcium within C-S-H. The O K-edge NEXAFS spectrum for C_3S hydration in the presence of $CaCl_2$ indicates that O K-edge NEXAFS is also very useful for distinguishing the chemical components in hydrated C_3S.

The chemical component mapping based on Ca $L_{3,2}$-edge and O K-edge NEXAFS spectra and image stacks reveals that the hydration product for C-S-H surrounds the unhydrated C_3S, along with the formation of $Ca(OH)_2$ in 7-day-hydrated C_3S in the presence of $CaCl_2$. However, $CaCl_2$ coexists not with C-S-H but with unhydrated C_3S. It is possible for $CaCl_2$ to accelerate the dissolution of ions from unhydrated C_3S, which results in increasing the hydration.

The network-cross fibrillary C-S-H gel was observed by STXM with Si K-edge NEXAFS spectra, whereas both the thin-sheet and the fibrillary C-S-H were also observed by SEM. $CaCl_2$ increases the degree of silicate polymerization.

The ^{29}Si MAS NMR analysis reveals that the presence of $CaCl_2$ in hydrated C_3S accelerates the formation of middle groups (Q^2) and branch sites (Q^3) in the silicate chains of C-S-H gel considerably, in agreement with increasing the degree of polymerization of the silicate chains in C-S-H gel considerably. $CaCl_2$ possibly prompts the bridge of the dreierketten silicate chains of C-S-H to develop in the two-dimensional direction into crumpled-foil C-S-H.

These findings definitely validate the STXM with NEXAFS spectra as a significantly powerful tool for investigating the microstructure of cementitious pastes, thus opening the possibility of studying the *in situ* nanostructure of cementitious materials during hydration.

Conflict of Interests

The authors declare that there is no conflict of interests regarding the publication of this paper.

Acknowledgments

STXM data were acquired at beamline BL5.3.2.1 and beamline BL5.3.2.2 at the Advanced Light Source, supported by the Director of the Office of Science, Office of Basic Energy Sciences of the US Department of Energy, under Contract no. DE-AC02-05CH11231. Funding for this project was provided by the National Natural Science Foundation of China (no. 51278157).

References

[1] J. J. Thomas, A. J. Allen, and H. M. Jennings, "Hydration kinetics and microstructure development of normal and $CaCl_2$-accelerated tricalcium silicate pastes," *Journal of Physical Chemistry C*, vol. 113, no. 46, pp. 19836–19844, 2009.

[2] M. C. G. Juenger, P. J. M. Monteiro, E. M. Gartner, and G. P. Denbeaux, "A soft X-ray microscope investigation into the effects of calcium chloride on tricalcium silicate hydration," *Cement and Concrete Research*, vol. 35, no. 1, pp. 19–25, 2005.

[3] P. K. Mehta and P. J. M. Monteiro, *Concrete: Microstructure, Properties, and Materials*, McGraw-Hill, New York, NY, USA, 4th edition, 2014.

[4] V. K. Peterson and A. E. Whitten, "Hydration processes in tricalcium silicate: application of the boundary nucleation model to quasielastic neutron scattering data," *Journal of Physical Chemistry C*, vol. 113, no. 6, pp. 2347–2351, 2009.

[5] E. M. Gartner, J. F. Young, D. A. Damidot, and I. Jawed, "Hydration of portland cement," in *The Structure and Performance of Cements*, J. Bensted and P. Barnes, Eds., chapter 3, Spon Press, London, UK, 2nd edition, 2002.

[6] M. C. G. Juenger and H. M. Jennings, "The use of nitrogen adsorption to assess the microstructure of cement paste," *Cement and Concrete Research*, vol. 31, no. 6, pp. 883–892, 2001.

[7] J. Skalny, I. Odler, and J. Hagymassy Jr., "Pore structure of hydrated calcium silicates. I. Influence of calcium chloride on the pore structure of hydrated tricalcium silicate," *Journal of Colloid And Interface Science*, vol. 35, no. 3, pp. 434–440, 1971.

[8] E. M. Gartner, K. E. Kurtis, and P. J. M. Monteiro, "Proposed mechanism of C-S-H growth tested by soft X-ray microscopy," *Cement and Concrete Research*, vol. 30, no. 5, pp. 817–822, 2000.

[9] V. S. Ramachandran and R. F. Feldman, "Time-dependent and intrinsic characteristics of portland cement hydrated in the presence of calcium chloride," *Il Cemento*, vol. 3, 1978.

[10] A. M. Rosenberg, "Study of the mechanism through which calcium chloride accelerates the set of portland cement," *Journal of American Concrete Institute*, vol. 61, pp. 1261–1269, 1964.

[11] G. W. Groves, P. J. Le Sueur, and W. Sinclair, "Transmission electron microscopy and microanalytical studies of ion-beam-thinned sections of tricalcium silicate paste," *Journal of the American Ceramic Society*, vol. 69, no. 4, pp. 353–356, 1986.

[12] K. E. Kurtis, P. J. M. Monteiro, J. T. Brown, and W. Meyer-Ilse, "High resolution transmission soft X-ray microscopy of deterioration products developed in large concrete dams," *Journal of Microscopy*, vol. 196, no. 3, pp. 288–298, 1999.

[13] K. E. Kurtis, P. J. M. Monteiro, J. T. Brown, and W. Meyer-Ilse, "Imaging of ASR gel by soft X-ray microscopy," *Cement and Concrete Research*, vol. 28, no. 3, pp. 411–421, 1998.

[14] J. Ha, S. Chae, K. W. Chou, T. Tyliszczak, and P. J. M. Monteiro, "Effect of polymers on the nanostructure and on the carbonation of calcium silicate hydrates: a scanning transmission X-ray microscopy study," *Journal of Materials Science*, vol. 47, no. 2, pp. 976–989, 2012.

[15] J. Ha, S. Chae, K. W. Chou, T. Tyliszczak, and P. J. M. Monteiro, "Scanning transmission X-ray microscopic study of carbonated calcium silicate hydrate," *Transportation Research Record*, vol. 2142, pp. 83–88, 2010.

[16] S. R. Chae, J. Moon, S. Yoon et al., "Advanced nanoscale characterization of cement based materials using X-ray synchrotron radiation: a review," *International Journal of Concrete Structures and Materials*, vol. 7, no. 2, pp. 95–110, 2013.

[17] P. J. M. Monteiro, L. Clodic, F. Battocchio et al., "Incorporating carbon sequestration materials in civil infrastructure: a micro and nano-structural analysis," *Cement and Concrete Composites*, vol. 40, pp. 14–20, 2013.

[18] D. Hernández-Cruz, C. W. Hargis, S. Bae et al., "Multiscale characterization of chemical—mechanical interactions between polymer fibers and cementitious matrix," *Cement and Concrete Composites*, vol. 48, pp. 9–18, 2014.

[19] S. Yoon, J. Ha, S. R. Chae, D. A. Kilcoyne, and P. J. M. Monteiro, "X-ray spectromicroscopic study of interactions between NaCl

and calcium silicate hydrates," *Magazine of Concrete Research*, vol. 66, no. 3, pp. 141–149, 2014.

[20] G. Johansson, J. Dynes, A. Hitchcock, T. Tyliszczak, G. Swerhone, and J. Lawrence, "Chemically sensitive tomography at 50 nm spatial resolution using a soft X-ray scanning transmission X-ray microscope," *Microscopy and Microanalysis*, vol. 12, supplement S02, pp. 1412–1413, 2006.

[21] Z. Yangquanwei, S. Neethirajan, and C. Karunakaran, "Cytogenetic analysis of quinoa chromosomes using nanoscale imaging and spectroscopy techniques," *Nanoscale Research Letters*, vol. 8, no. 1, article 463, 7 pages, 2013.

[22] S. Bae, R. Taylor, D. Hernández-Cruz, S. Yoon, D. Kilcoyne, and P. J. M. Monteiro, "Soft X-ray spectromicroscopic investigation of synthetic C-S-H and C_3S hydration products," *Journal of the American Ceramic Society*, vol. 98, no. 9, pp. 2914–2920, 2015.

[23] A. L. D. Kilcoyne, T. Tyliszczak, W. F. Steele et al., "Interferometer-controlled scanning transmission X-ray microscopes at the Advanced Light Source," *Journal of Synchrotron Radiation*, vol. 10, no. 2, pp. 125–136, 2003.

[24] S. J. Naftel, T. K. Sham, Y. M. Yiu, and B. W. Yates, "Calcium *L*-edge XANES study of some calcium compounds," *Journal of Synchrotron Radiation*, vol. 8, no. 2, pp. 255–257, 2001.

[25] F. M. F. de Groot, J. C. Fuggle, B. T. Thole, and G. A. Sawatzky, "2*p* x-ray absorption of 3*d* transition-metal compounds: an atomic multiplet description including the crystal field," *Physical Review B: Condensed Matter and Materials Physics*, vol. 42, no. 9, pp. 5459–5468, 1990.

[26] R. T. DeVol, R. A. Metzler, L. Kabalah-Amitai et al., "Oxygen spectroscopy and polarization-dependent imaging contrast (PIC)-mapping of calcium carbonate minerals and biominerals," *Journal of Physical Chemistry B*, vol. 118, no. 28, pp. 8449–8457, 2014.

[27] T. Nagai, T. Ito, T. Hattori, and T. Yamanaka, "Compression mechanism and amorphization of portlandite, $Ca(OH)_2$: structural refinement under pressure," *Physics and Chemistry of Minerals*, vol. 27, no. 7, pp. 462–466, 2000.

[28] H. W. F. Taylor, *Cement Chemistry*, Thomas Telford, London, UK, 2nd edition, 1997.

[29] D. Li, G. M. Bancroft, M. E. Fleet, and X. H. Feng, "Silicon K-edge XANES spectra of silicate minerals," *Physics and Chemistry of Minerals*, vol. 22, no. 2, pp. 115–122, 1995.

[30] J. J. Thomas, H. M. Jennings, and J. J. Chen, "Influence of nucleation seeding on the hydration mechanisms of tricalcium silicate and cement," *Journal of Physical Chemistry C*, vol. 113, no. 11, pp. 4327–4334, 2009.

[31] N. B. Singh and P. N. Ojha, "Effect of $CaCl_2$ on the hydration of tricalcium silicate," *Journal of Materials Science*, vol. 16, no. 10, pp. 2675–2681, 1981.

[32] J. F. Young, R. L. Berger, and F. V. Lawrence Jr., "Studies on the hydration of tricalcium silicate pastes III. Influence of admixtures on hydration and strength development," *Cement and Concrete Research*, vol. 3, no. 6, pp. 689–700, 1973.

[33] J. J. Beaudoin, L. Raki, and R. Alizadeh, "A ^{29}Si MAS NMR study of modified C-S-H nanostructures," *Cement and Concrete Composites*, vol. 31, no. 8, pp. 585–590, 2009.

[34] M. Chloup-Bondant and O. Evrard, "Tricalcium aluminate and silicate hydration. Effect of limestone and calcium sulfate," in *Nuclear Magnetic Resonance Spectroscopy of Cement-Based Materials*, P. Colombet, H. Zanni, A.-R. Grimmer, and P. Sozzani, Eds., pp. 295–308, Springer, Berlin, Germany, 1998.

[35] S. A. Rodger, G. W. Groves, N. J. Clayden, and C. M. Dobson, "Hydration of tricalcium silicate followed by ^{29}Si NMR with cross-polarization," *Journal of the American Ceramic Society*, vol. 71, no. 2, pp. 91–96, 1988.

[36] M. Mägi, E. Lippmaa, A. Samoson, G. Engelhardt, and A.-R. Grimmer, "Solid-state high-resolution silicon-29 chemical shifts in silicates," *Journal of Physical Chemistry*, vol. 88, no. 8, pp. 1518–1522, 1984.

[37] C. E. Tambelli, J. F. Schneider, N. P. Hasparyk, and P. J. M. Monteiro, "Study of the structure of alkali-silica reaction gel by high-resolution NMR spectroscopy," *Journal of Non-Crystalline Solids*, vol. 352, no. 32–35, pp. 3429–3436, 2006.

[38] R. J. Myers, S. A. Bernal, R. San Nicolas, and J. L. Provis, "Generalized structural description of calcium-sodium aluminosilicate hydrate gels: the cross-linked substituted tobermorite model," *Langmuir*, vol. 29, no. 17, pp. 5294–5306, 2013.